ARMY RESEARCH LABORATORY

Calibrated Mid-wave Infrared (IR) (MidIR) and Long-wave IR (LWIR) Stokes and Degree-of-Liner Polarization (DOLP)

by Kristan P. Gurton and Melvin Felton

ARL-TR-4544 **September 2008**

NOTICES

Disclaimers

The findings in this report are not to be construed as an official Department of the Army position unless so designated by other authorized documents.

Citation of manufacturer's or trade names does not constitute an official endorsement or approval of the use thereof.

Destroy this report when it is no longer needed. Do not return it to the originator.

Army Research Laboratory
Adelphi, MD 20783-1197

ARL-TR-4544 **September 2008**

Calibrated Mid-wave Infrared (IR) (MidIR) and Long-wave IR (LWIR) Stokes and Degree-of-Liner Polarization (DOLP)

Kristan P. Gurton and Melvin Felton
Computational and Information Sciences Directorate, ARL

REPORT DOCUMENTATION PAGE

Form Approved
OMB No. 0704-0188

1. REPORT DATE *(DD-MM-YYYY)*	2. REPORT TYPE	3. DATES COVERED (From - To)
September 2008	Final	

4. TITLE AND SUBTITLE
Calibrated Mid-wave Infrared (IR) (MidIR) and Long-wave IR (LWIR) Stokes and Degree-of-Liner Polarization (DOLP)

5a. CONTRACT NUMBER

5b. GRANT NUMBER

5c. PROGRAM ELEMENT NUMBER

6. AUTHOR(S)
Kristan P. Gurton and Melvin Felton

5d. PROJECT NUMBER

5e. TASK NUMBER

5f. WORK UNIT NUMBER

7. PERFORMING ORGANIZATION NAME(S) AND ADDRESS(ES)
U.S. Army Research Laboratory
Computational and Information Sciences Directorate
Atmospheric Sensing Branch (ATTN: AMSRD-ARL-CI-ES)
Adelphi, MD 20783-1197

8. PERFORMING ORGANIZATION REPORT NUMBER
ARL-TR-4544

9. SPONSORING/MONITORING AGENCY NAME(S) AND ADDRESS(ES)

10. SPONSOR/MONITOR'S ACRONYM(S)

11. SPONSOR/MONITOR'S REPORT NUMBER(S)

12. DISTRIBUTION/AVAILABILITY STATEMENT
Approved for public release; distribution is unlimited.

13. SUPPLEMENTARY NOTES

14. ABSTRACT
We present radiometric and polarimetric calibrated imagery recorded in both the mid-wave infrared (IR) (MidIR) and long-wave IR (LWIR) as a function of diurnal variation over several multiday periods. We compare differences in polarimetric and conventional thermal imagery for both IR atmospheric transmission windows, i.e., the 3–5 μm and 8–12 μm regions. Meteorological parameters measured during the study include temperature, relative humidity, wind speed/direction, precipitation, and ambient atmospheric IR loading. The two camera systems used in the study differed significantly in design. The LWIR polarimetric sensor utilizes a spinning achromatic retarder and is best suited for static scenes, while the MidIR system is based on a division-of-aperture design and is capable of recording polarimetric imagery of targets that are rapidly moving. Examples of both S_0 (conventional thermal) and degree-of-linear polarization (DOLP) imagery are presented and compared.

15. SUBJECT TERMS
Polarimetric, MidIR, LWIR stokes, DOLP, imagery

16. SECURITY CLASSIFICATION OF:			17. LIMITATION OF ABSTRACT	18. NUMBER OF PAGES	19a. NAME OF RESPONSIBLE PERSON
a. REPORT	b. ABSTRACT	c. THIS PAGE			Kristan P. Gurton
U	U	U	UU	30	19b. TELEPHONE NUMBER (*Include area code*) (301) 394-2093

Standard Form 298 (Rev. 8/98)
Prescribed by ANSI Std. Z39.18

Contents

List of Figures

List of Tables

Summary

Atmospheric conditions are known to have an effect on the polarimetric signature of objects. We present radiometric and polarimetric calibrated imagery recorded in both the mid-wave infrared (IR) (MidIR) and long-wave IR (LWIR) as a function of diurnal variation over several multiday periods. The two camera systems used in the study differed significantly in design. The LWIR (8–14 μm) polarimetric sensor utilizes a spinning achromatic retarder, while the MidIR (3–5 μm) system is based on a division-of-aperture design. Within the respective wavebands, average values for the intensity of the radiation and the degree of linear polarization for various scenes were used in the analysis. In addition, the meteorological parameters measured during the study included temperature, relative humidity, wind speed/direction, precipitation, and ambient atmospheric IR loading. It was observed that the polarimetric signatures of the objects in this study varied more in MidIR than in the LWIR. In addition, it was observed that these variations were inversely correlated to relative humidity and greatly affected by periods of rain. These results suggest that if relatively stable polarimetric signatures are desired, then the LWIR is the suitable waveband to choose.

INTENTIONALLY LEFT BLANK.

1. Introduction

We present a study designed to quantify the variance in a popular polarimetric metric, the degree-of-linear polarization (DOLP), in both the mid-wave infrared (IR) (MidIR) and long-wave IR (LWIR) waveband regions that are recorded within an urban environment as a function of temperature, relative humidity, and ambient thermal loading (i.e., the integrated radiance from 3–50 μm). The test was conducted in a large concrete parking lot located between two large three-story buildings in Adelphi, MD. Target objects were chosen to include a variety of manmade materials such as glass, roughened painted metal, wood, a polyurethane-based tarp/tent, and the concrete surface of the lot itself. All targets remained fixed in place during the test. In addition, because of their relative close proximity to each other (and the surrounding buildings), targets were subject to the type of radiant loading most associated to an urban environment, i.e., target signatures determined by both self and reflected emission (figure 1).

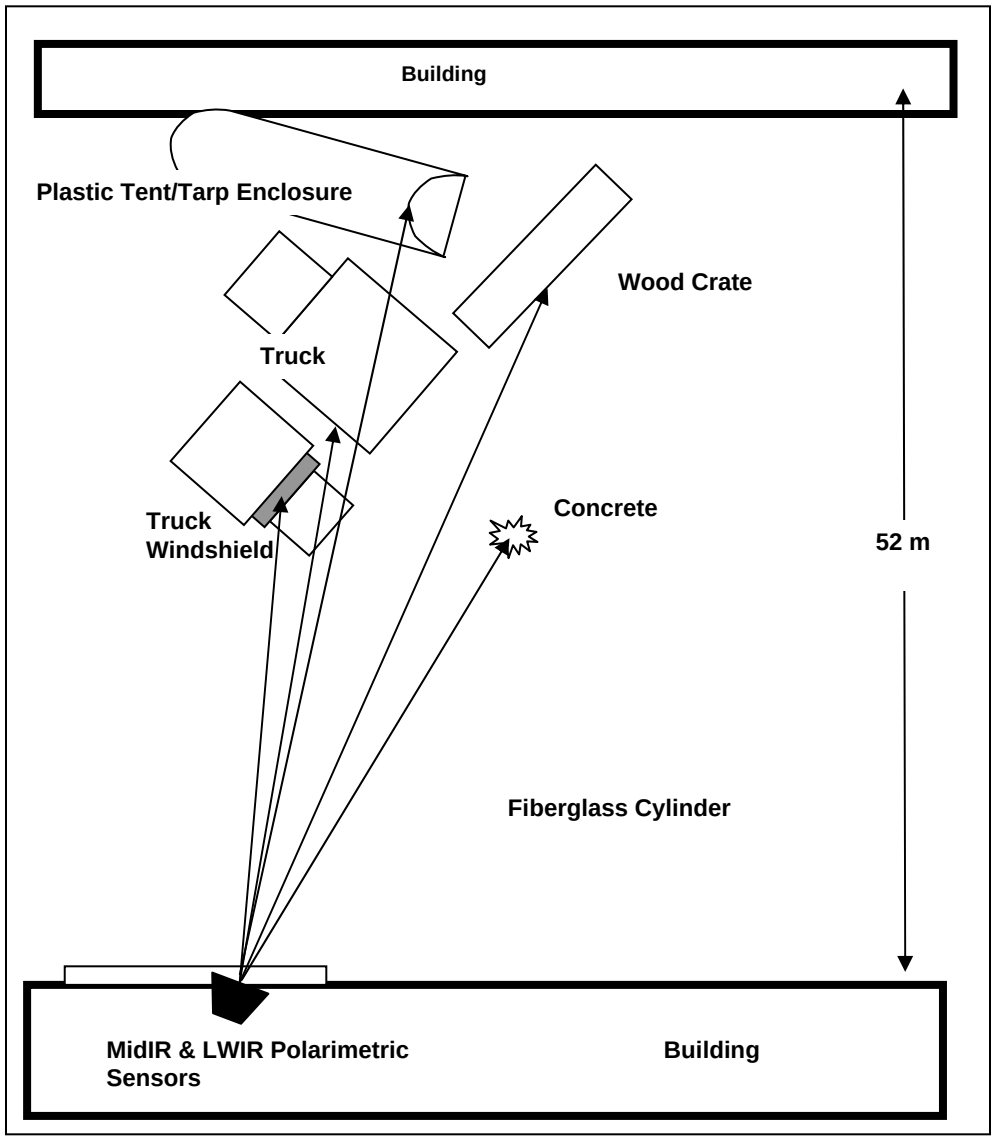

Figure 1. Sample schematic of test parking lot.

Polarimetric data (imagry) was recorded with a set of prototype thermal polarimetric sensors, one designed for MidIR and one designed for LWIR operation, produced by Polaris Sensors Technologies Inc., Huntsville, AL. Although both systems were purchased from Polaris Sensors Technologies, they differed very significantly in optical design and operation.

The MidIR camera system is based on a division-of-aperture (DOA) approach in which the scene entering the objective is split evenly into four different optical paths. Each path is then projected onto one of four quadrants that make up the 640x512 focal-plane array (FPA). A wire-grid polarizer is placed in each of the four optical paths (oriented at 0°, 90°, and ±45°, respectively) and serves to filter the image forming radiance. The image quadrants are recorded and then combined in a variety of user defined algebraic combinations allowing, for example, the calculation of the Stokes-vector images. These processed images are obtained simultaneously

during the recording of a single frame and any one of them may be chosen to be displayed in a nearly real-time manner. As a result, the DOA approach is well suited for recording scenes in which the target of interest is rapidly moving (*1*).

Conversely, whereas the DOA approach (used in the MidIR system) generates polarimetric products from a single frame, the LWIR camera system is based on a rapidly spinning achromatic retarder design that generates a sequence of polarimetric images on each revolution of the retarder that are stored and processed into the conventional Stokes images S_0, S_1, S_2, and S_3. The obvious disadvantage to this approach is that for highly dynamic scenes, misregistration between pixel locations within sequential frames may occur. However, operating at a maximum frame rate of 240 Hz (with images windowed down to 152x158 pixels) with the speed of the spinning wave plate set at 8 rps, the Stokes video is recorded at 30 Hz and we rarely observe moving targets in the field that exhibit large misregistration artifacts.

A series of polarimetric images were recorded approximately every 30 min with the camera system(s) oriented at one of three different scenes in order to sample a wide variety of materials. Each camera was fitted with a 50 mm IR objective lens. Because of the differing FPA dimensions and optical paths inherent to each camera (152x158 pixels for the mercury cadmium telluride (MCT) based LWIR sensor, and 220x220 pixels for each quadrant of the indium antimonide (InSb) based MidIR sensor), slightly different fields-of-view (FOVs) were sampled. As a result, FOVs for the LWIR and MidIR cameras using a 50 mm objective lens were 15° and 11°, respectively. Therefore, the instantaneous FOV for the LWIR and MidIR cameras is 0.1° and 0.05°, respectively.

A simple schematic of the test lot is shown in figure 1. As seen in the diagram two trucks are parked at an approximate 45° angle (with respect to the sides of the buildings), and regions of the trucks were sampled to generate “windshield” and “truck-side” DOLP and S_0 image cubes (figure 2). Similarly, objects shown in figure 2 used in the analysis include a wooden shipping crate, a region of the concrete parking lot, and the top portion of plastic tent/tarp enclosure.

The response for both sensors were optimized by setting the integration time and video-offset based upon the expected radiance values to be recorded in order to match the full dynamic range of their respective analog-to-digital (AD) frame-grabber response. Nonuniformity corrections (NUC) were conducted periodically by filling the FOV with the calibrated radiance from a 14 in. x 14 in. blackbody and served as the needed radiometric calibration for each camera.

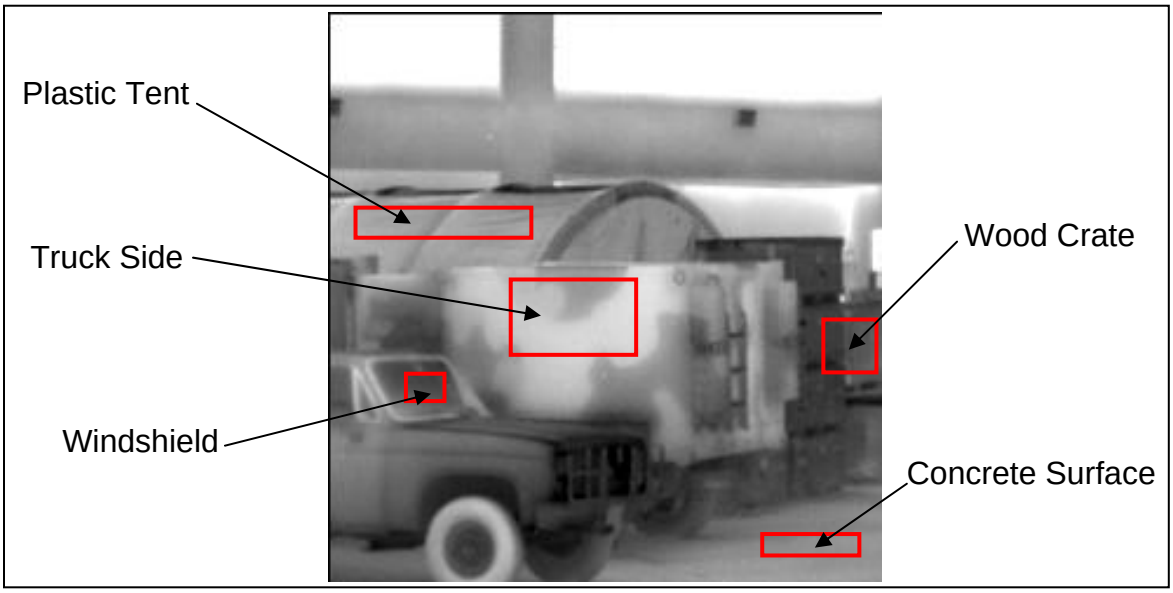

Figure 2. Sample MidIR S_0 image showing the various target areas, i.e., plastic tent, truck side, windshield, wood crate, and concrete parking lot surface.

Polarimetric calibration was accomplished by recording linearly polarized calibrated imagery at known polarization states. A 4.0 in. diameter barium fluoride (BaF_2) wire-grid polarizer was placed in front of the calibrated blackbody and thermal imagery was sequentially recorded with the polarizer oriented at 0°, 45°, 90°, and 135°. Great care was taken to ensure reflected radiance from the face of the BaF_2 polarizer was kept constant (and to a minimum) throughout the calibration process (figure 3). This was accomplished by canting the face of the polarizer in order to reflect the radiance generated by a large, black, roughened cold-plate that was kept at 0 °C via contact with a large ice bath.

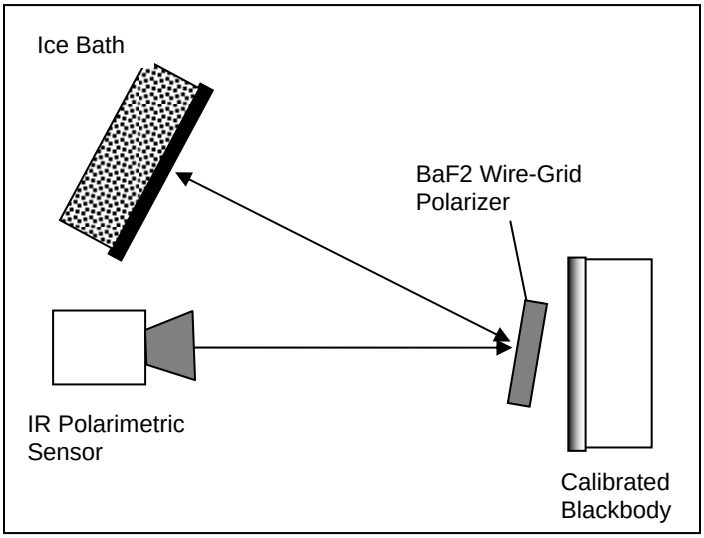

Figure 3. Controlling the reflected radiance during polarimetric calibration.

2. Environmental Conditions

Test periods were chosen during the two-week period from November 7 through November 14, 2007, in order to take advantage of changing meteorological conditions as several different weather patterns transitioned through the test area. Temperatures experienced at the test site ranged from a low of 0 °C (32 °F) to a high of 16 °C (61 °F), while relative humidity levels varied from a low of 58% to a high of 94%. Polarimetric imagry was recorded during periods that included a variety of atmospheric conditions such as clear sky, dense cloud cover, and rain (figure 4).

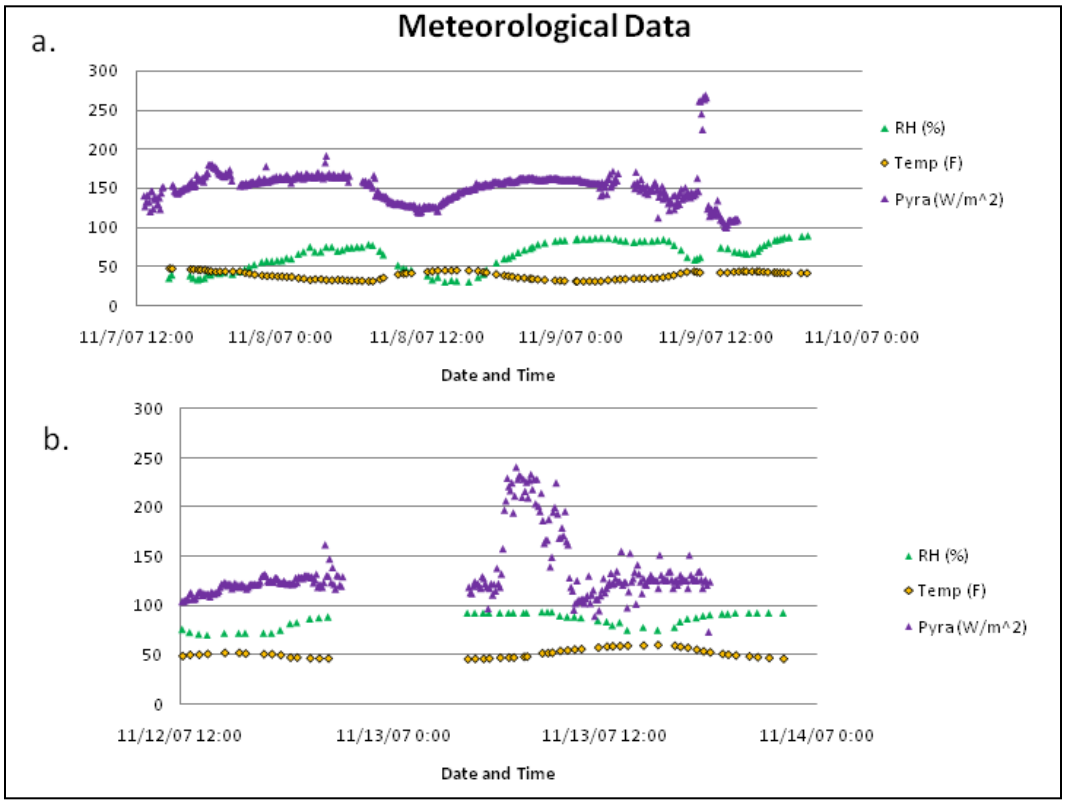

Figure 4. Diurnal plots of meteorological conditions for test periods: a. November 7–9, 2007 and b. November 12–13, 2007.

The ambient long-wave terrestrial radiation due to atmospheric emission, including reflected radiance from natural surfaces, was recorded continuously using an Eppley long-wave pyranometer. The long-wave pyranometer is designed to measure radiance from approximately 3 to 50 μm within a 2π steradian FOV and was positioned on top of an adjacent building in order to sample as much of the sky as possible.

3. Results

Polarimetric results are presented in figures 5–14 and tables 1–10, in which data points representing the DOLP where calculated by combining thermal images in the following manner:

$$S_0 = I(0) + I(90)\ (w/m^2), \tag{1}$$

$$S_1 = I(0) - I(90)\ (w/m^2), \tag{2}$$

$$S_2 = I(+45) - I(-45)\ (w/m^2), \tag{3}$$

$$\text{DOLP} = \frac{\sqrt{S_1^{\,2} + S_2^{\,2}}}{S_0}\ \text{(represented as a percentage)}, \tag{4}$$

where I(0), I(90), I(+45), and I(–45) represent images produced with radiance that is polarized vertical, horizontal, +45° from the vertical, and –45° from the vertical, respectively. Sets of either S_0 or DOLP images are then arranged in chronological order to form a given image cube. Regions-of-interest (ROI) within each cube are then identified, and a Z-profile containing average pixel values within each region is computed. Figure 2 is a sample image showing the various regions chosen.

As shown in figure 2 the sampled sets of surfaces can be broken into two groups based on the orientation of their surface normals. One group consists of surface normals that are not oriented toward the sky (i.e., the side of the truck and the surface of the stacked wooden crates) and the set of surfaces that are oriented more towards the sky (i.e., the windshield, plastic tent/tarp, and the concrete parking lot surface). Measured angles between a given surface normal and the line-of-sight (LOS) were found to be, 82°±2° for the sampled concrete surface, 22°±2° for the truck side, 77°±3° for the windshield, 58°±2° for the wood crate, and 62°±4° for the region of the plastic tent sampled.

Resultant S_0 and DOLP values extracted from the appropriate image cubes for the five materials are shown in figures 5 through 14 for the test periods conducted on either November 7–9 or November 12–13, 2007. Also shown are the resultant meteorological parameters as well as the ambient radiant loading experienced during the test recorded by the Eppley long-wave pyranometer. Tables 1 through 10 present a more concise “snapshot” of each period and material presented in tabular form in which hi, low, average, and standard deviation values of all parameters are shown.

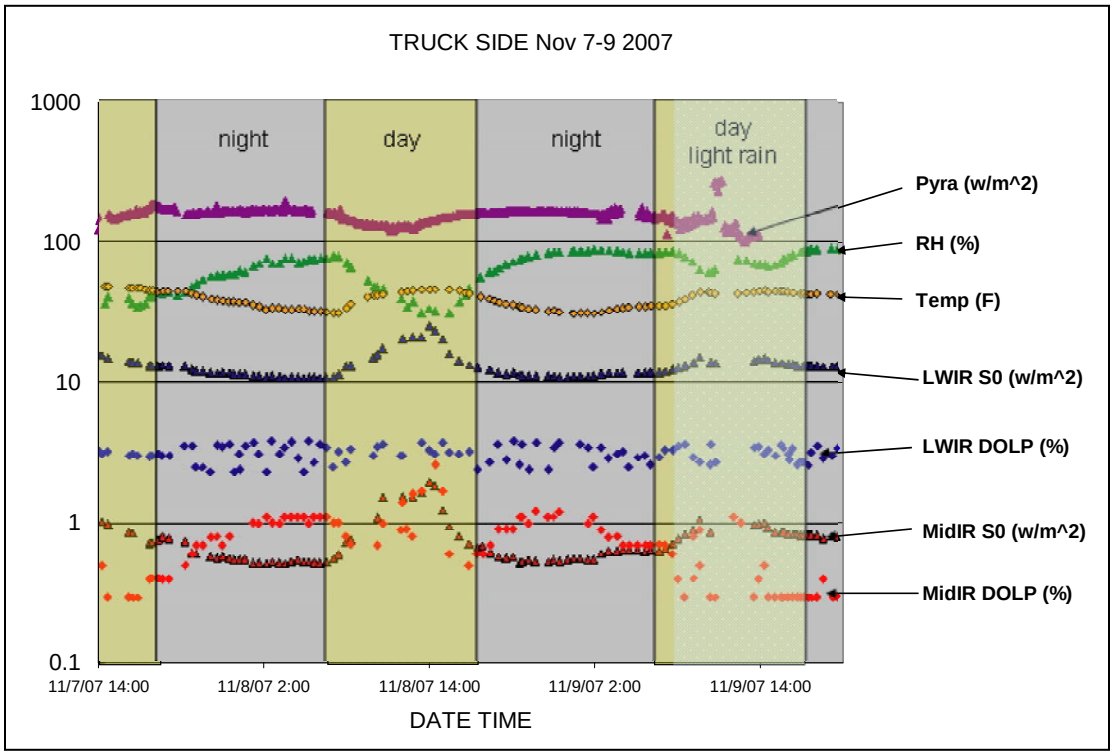

Figure 5. Diurnal plots for the truck side for the period November 7–9, 2007.

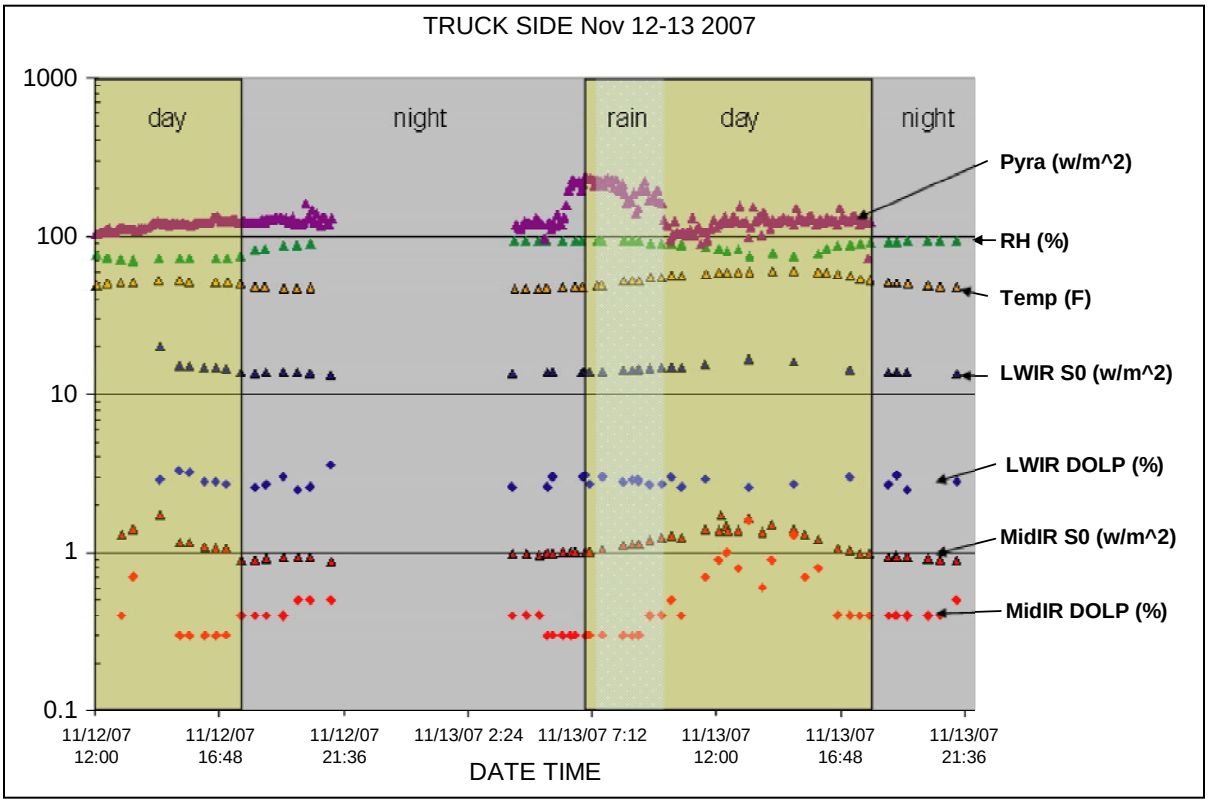

Figure 6. Diurnal plots for the truck side for the period November 12–13, 2007.

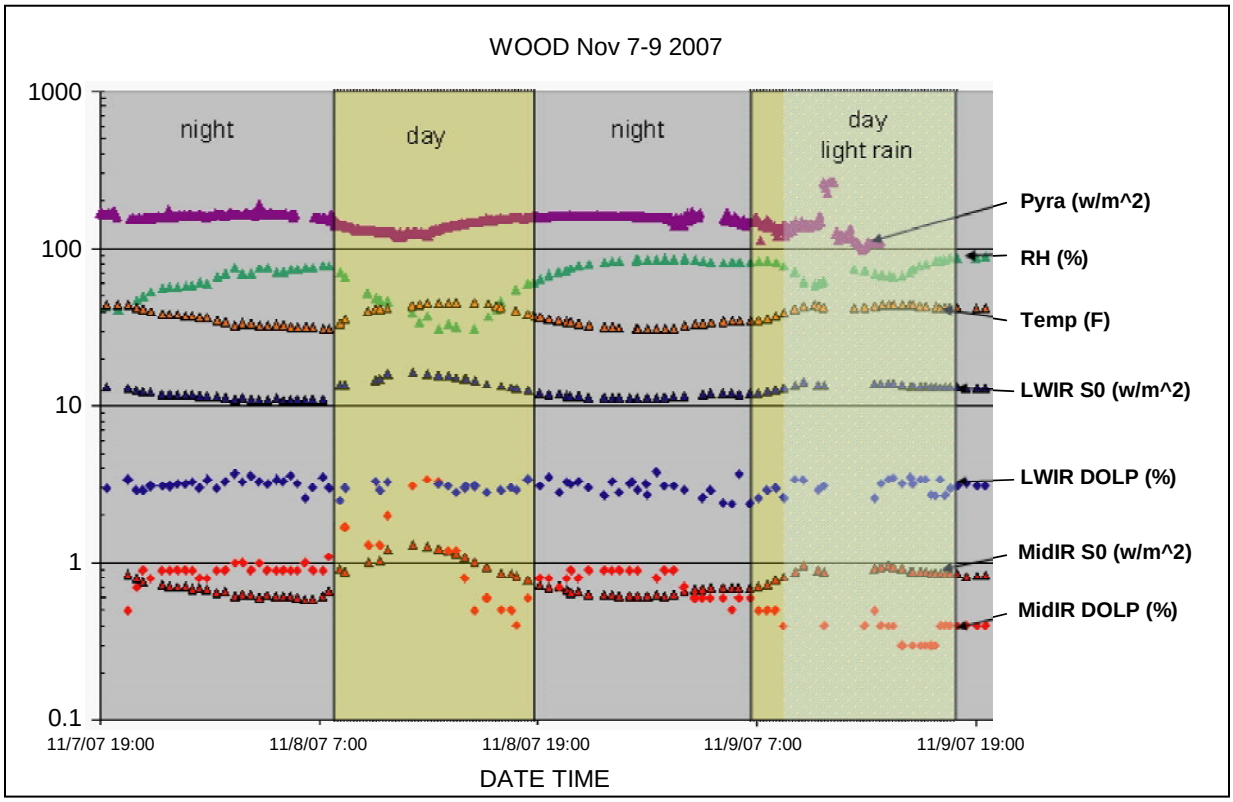

Figure 7. Diurnal plots for the wooden crate for the period November 7–9, 2007.

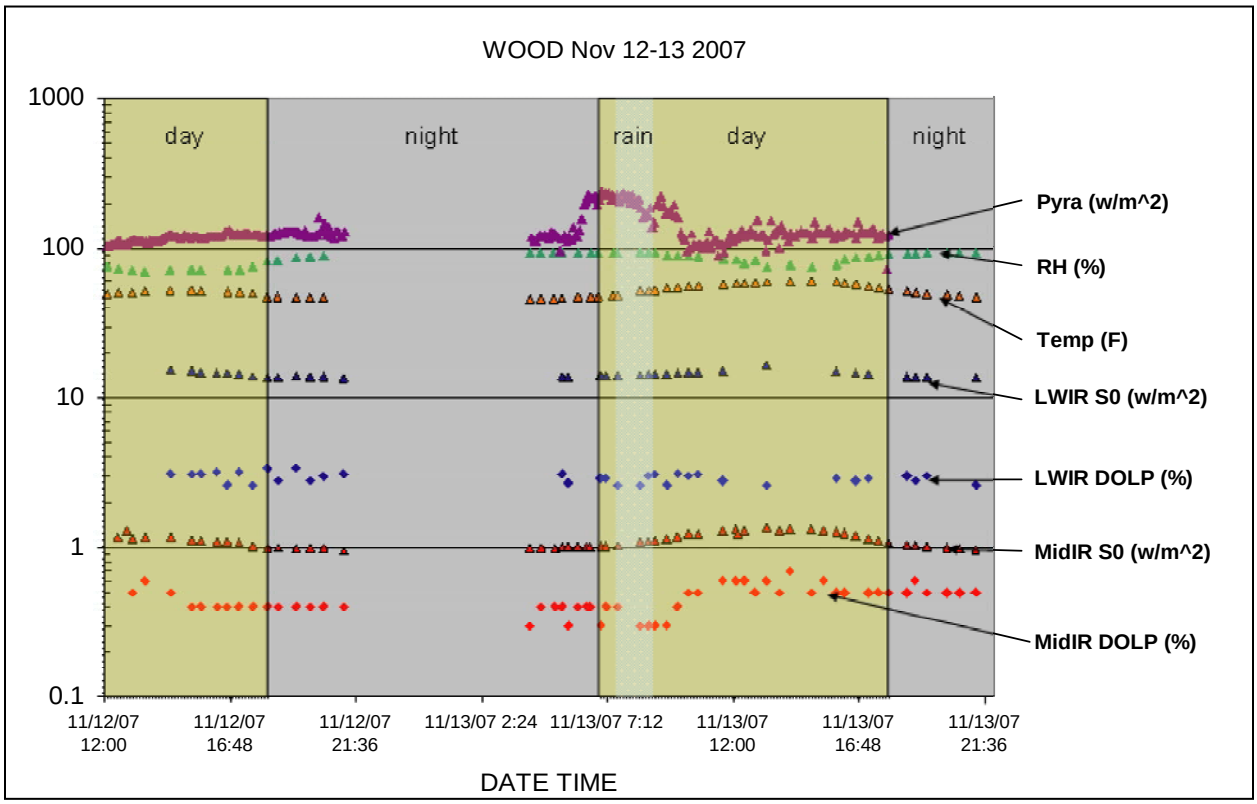

Figure 8. Diurnal plots for the wooden crate for the period November 12–13, 2007.

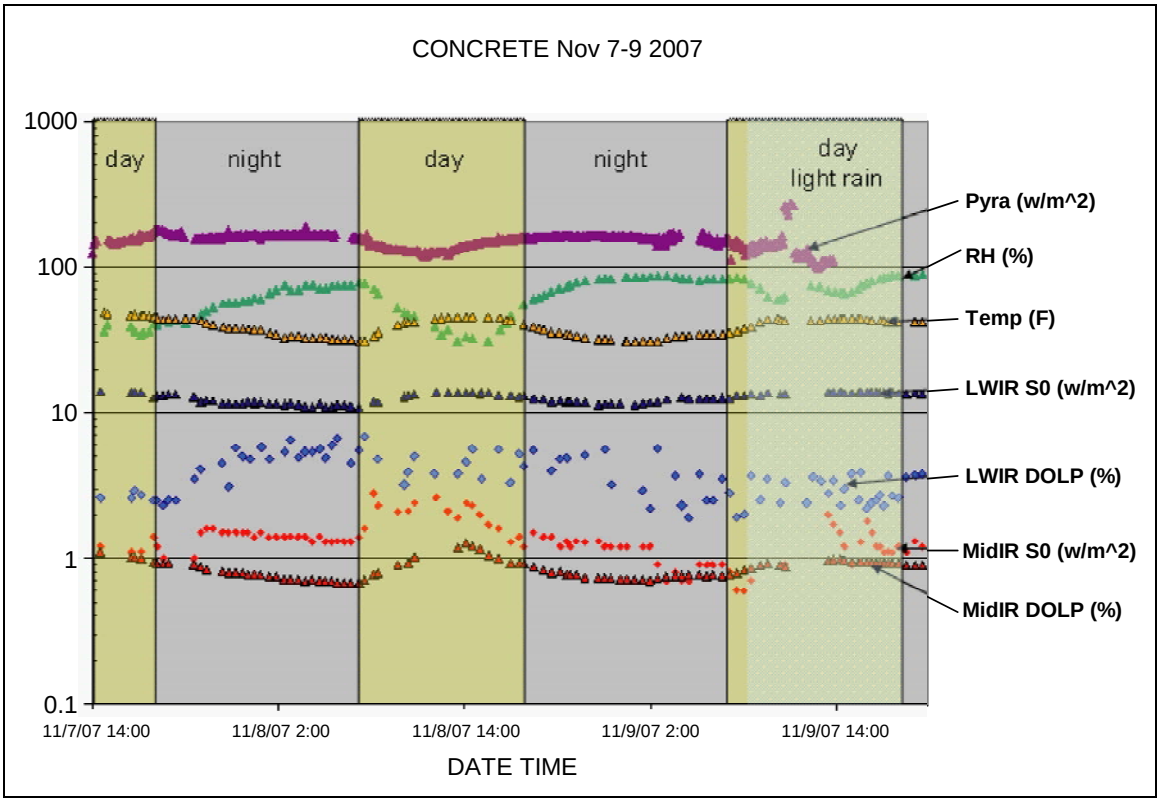

Figure 9. Diurnal plots for the concrete for the period November 7–9, 2007.

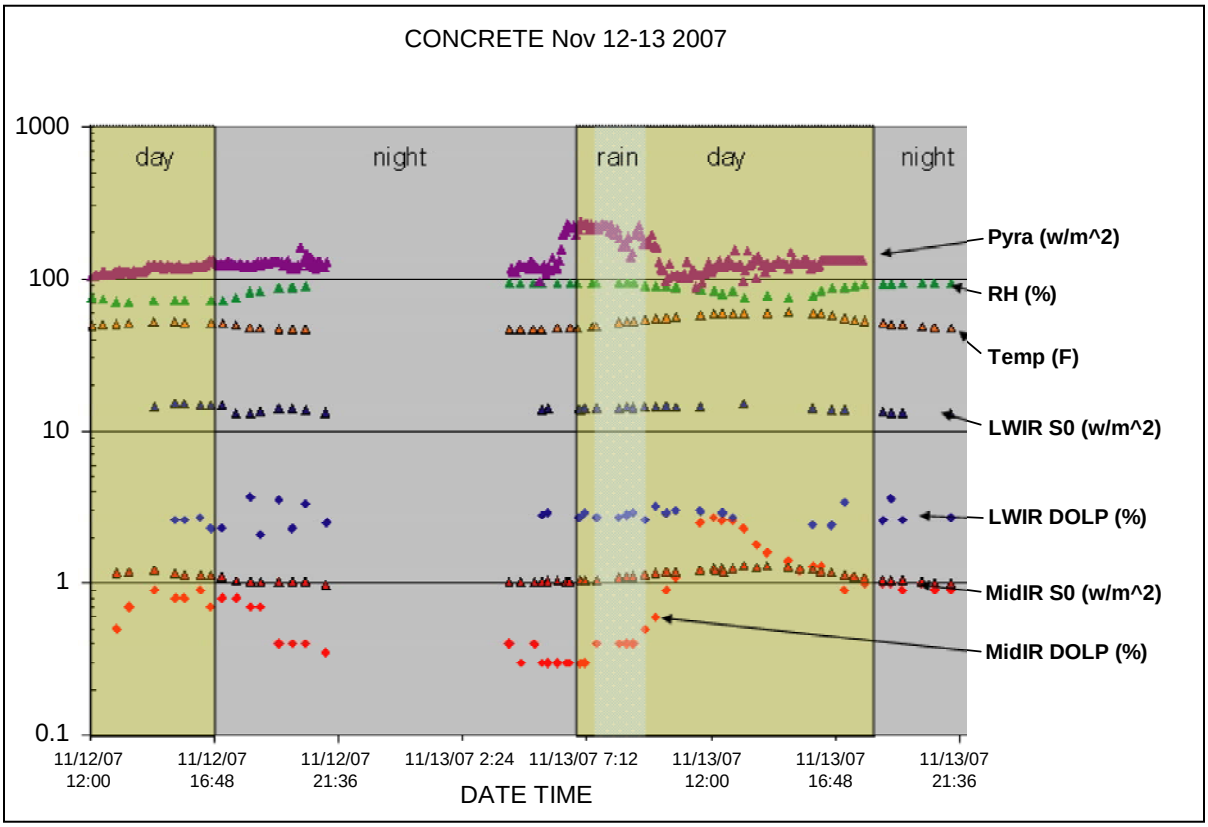

Figure 10. Diurnal plots for the concrete for the period November 12–13, 2007.

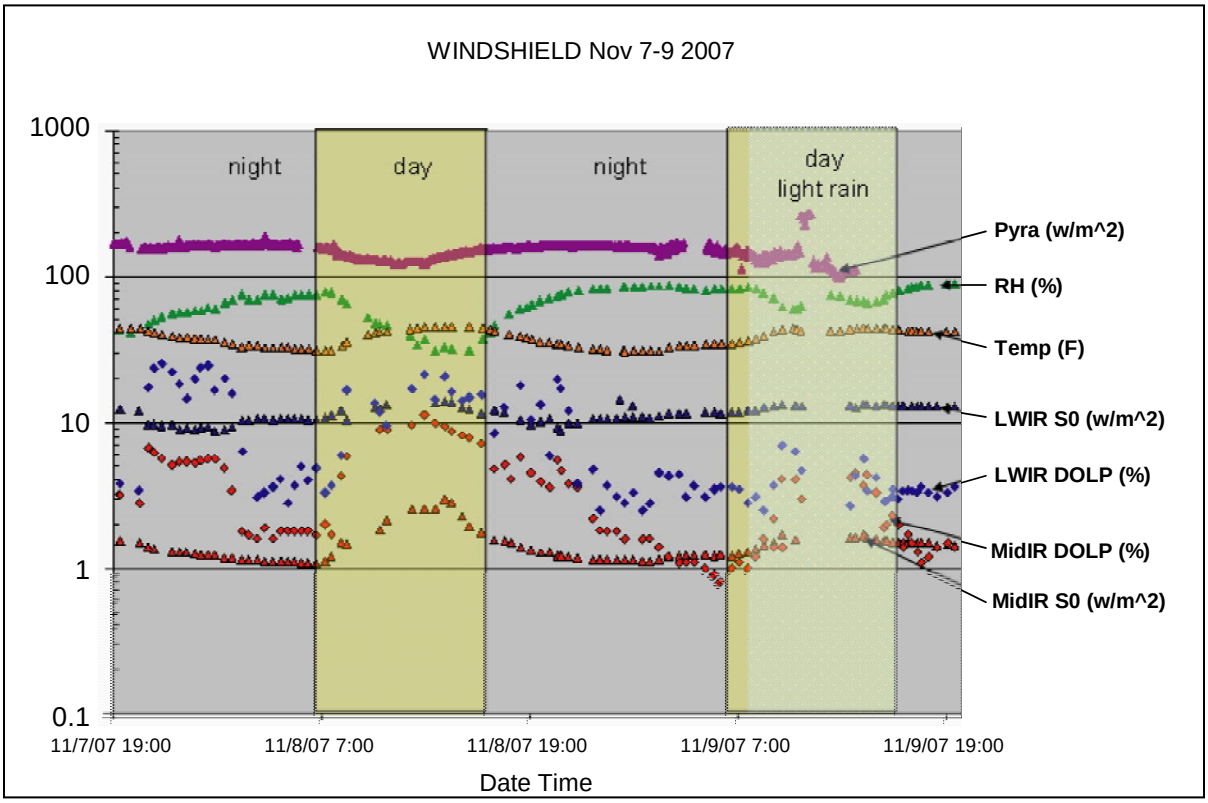

Figure 11. Diurnal plots for the windshield for the period November 7–9, 2007.

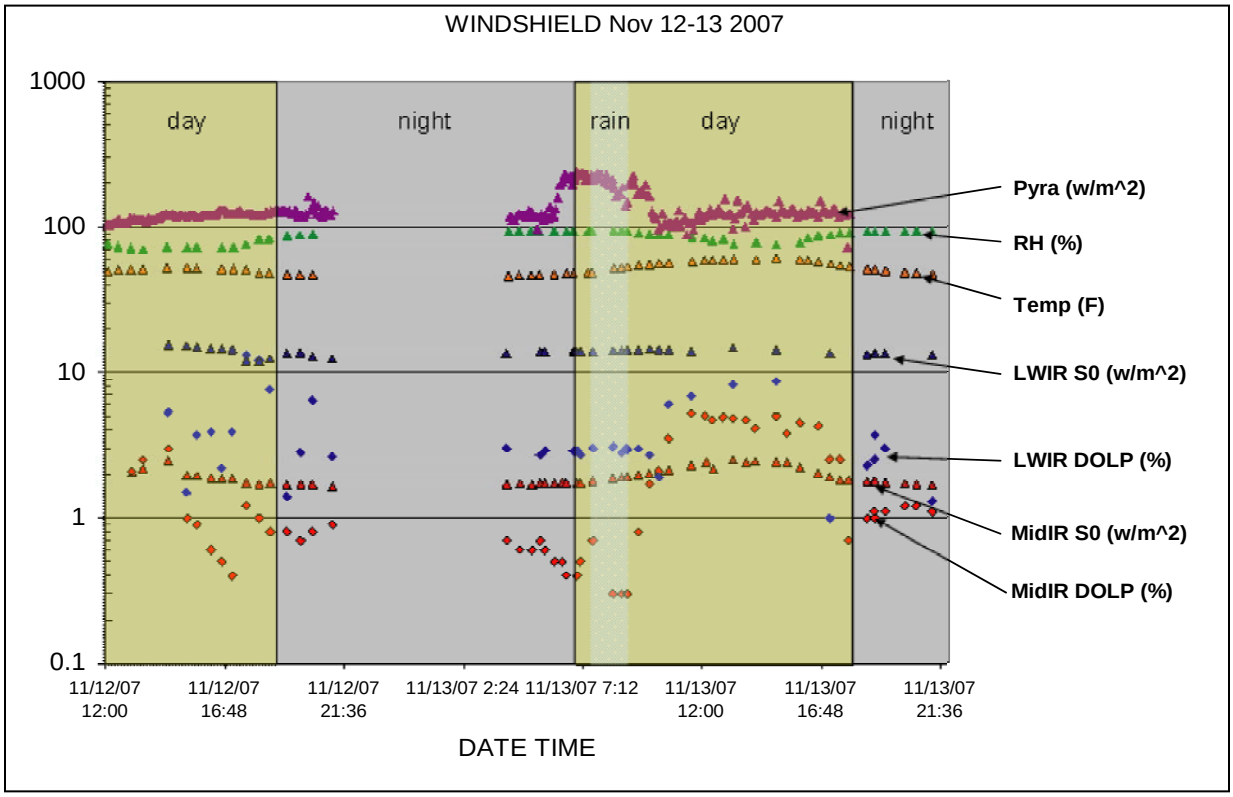

Figure 12. Diurnal plots for the windshield for the period November 12–13, 2007.

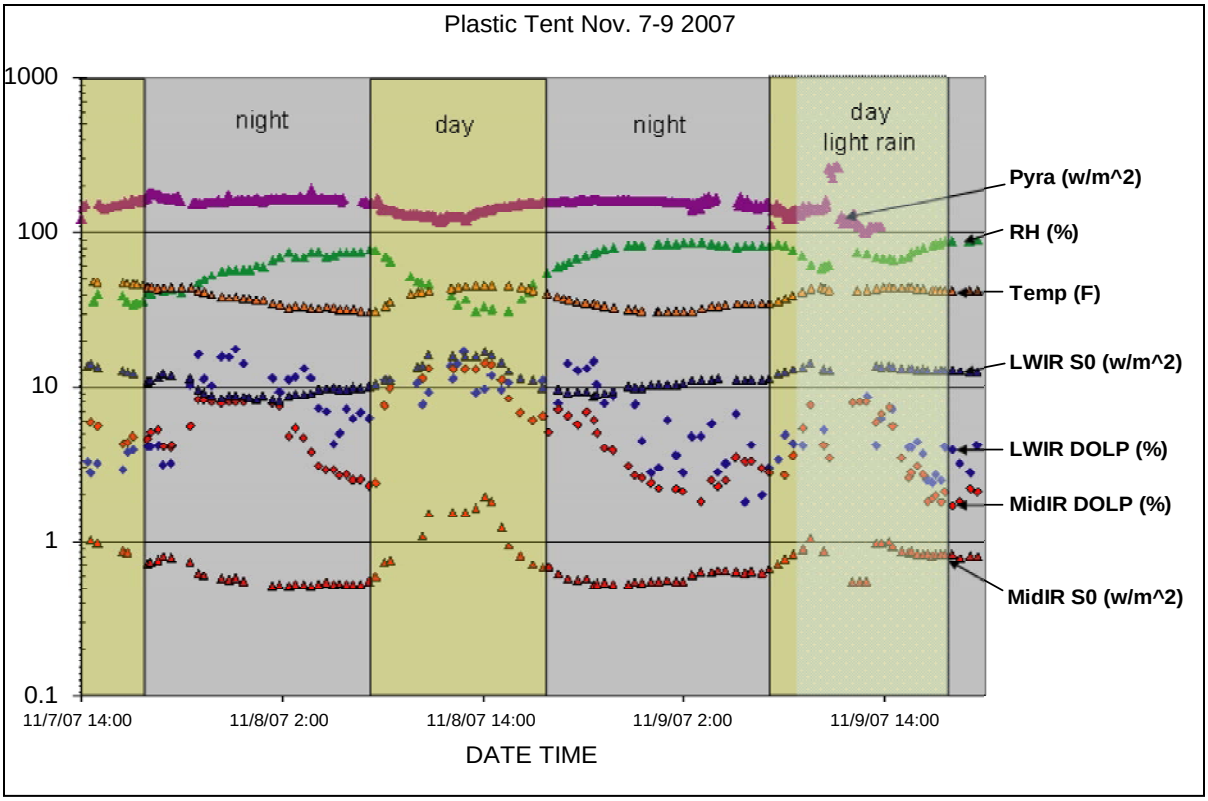

Figure 13. Diurnal plots for the tent for the period November 7–9, 2007.

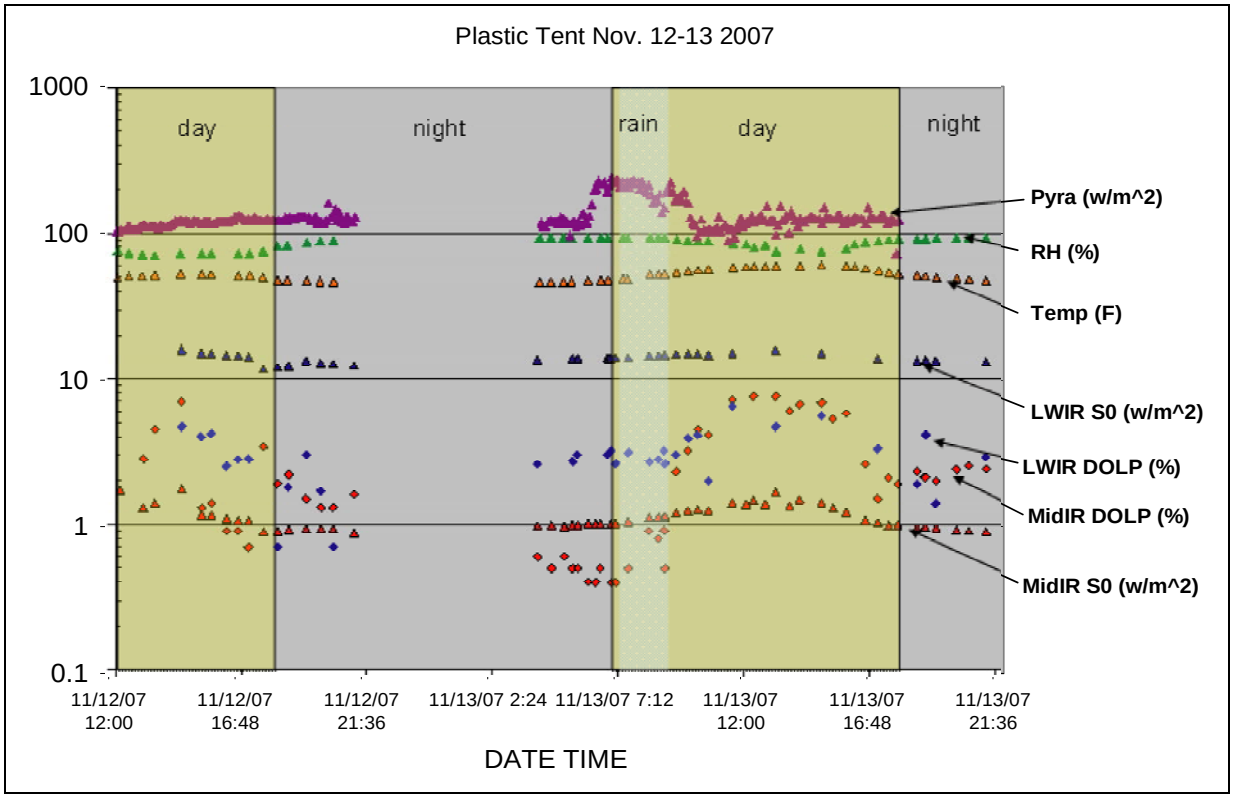

Figure 14. Diurnal plots for the tent for the period November 12–13, 2007.

Table 1. Statistical values for truck side for the period November 7–9, 2007.

Truck Side November 7–9 2007							
	LWIR DOLP (%)	**LWIR S0 (w/m^2)**	**MidIR DOLP (%)**	**MidIR S0 (w/m^2)**	**Atmospheric Radiation (w/m^2)**	**Temp. (°F)**	**Relative Humidity (%)**
Mean	3.11	13.01	0.74	0.76	151.44	38.76	64.43
Hi	3.8	24.95	2.6	1.95	268.54	48.02	89
Low	2.3	10.73	0.3	0.51	99.50	30.56	31
Standard Deviation	0.41	2.61	0.39	0.28	20.62	5.27	17.47

Table 2. Statistical values for the truck side for the period November 12–13, 2007.

Truck Side 12–13 2007							
	LWIR DOLP (%)	**LWIR S0 (w/m^2)**	**MidIR DOLP (%)**	**MidIR S0 (w/m^2)**	**Atmospheric Radiation (w/m^2)**	**Temp. (°F)**	**Relative Humidity (%)**
Mean	2.77	14.42	0.51	1.13	133.21	51.51	85.28
Hi	3.6	20.10	1.6	1.74	240.05	60.26	94
Low	0	13.28	0.3	0.88	72.60	43.52	70
Standard Deviation	0.51	1.19	0.30	0.22	32.49	4.53	8.06

Table 3. Statistical values for the wooden crate for the period November 7–9, 2007.

Wood November 7–9 2007							
	LWIR DOLP (%)	**LWIR S0 (w/m^2)**	**MidIR DOLP (%)**	**MidIR S0 (w/m^2)**	**Atmospheric Radiation (w/m^2)**	**Temp. (°F)**	**Relative Humidity (%)**
Mean	3.09	12.68	0.80	0.80	151.32	38.76	64.43
Hi	3.8	16.33	3.4	1.30	268.32	48.02	89
Low	2.4	10.87	0.3	0.59	99.42	30.56	31
Standard Deviation	0.29	1.34	0.54	0.17	20.60	5.27	17.47

Table 4. Statistical values for the wooden crate for the period November 12–13, 2007.

Wood November 12–13 2007							
	LWIR DOLP (%)	**LWIR S0 (w/m^2)**	**MidIR DOLP (%)**	**MidIR S0 (w/m^2)**	**Atmospheric Radiation (w/m^2)**	**Temp. (°F)**	**Relative Humidity (%)**
Mean	2.91	14.36	0.47	1.11	133.10	51.51	85.28
Hi	3.4	16.50	1	1.36	239.85	60.26	94
Low	2.5	13.52	0.3	0.92	167.31	43.52	70
Standard Deviation	0.23	0.63	0.12	0.12	32.46	4.53	8.06

Table 5. Statistical values for the concrete for the period November 7–9, 2007.

Concrete November 7–9 2007							
	LWIR DOLP (%)	**LWIR S0 (w/m^2)**	**MidIR DOLP (%)**	**MidIR S0 (w/m^2)**	**Atmospheric Radiation (w/m^2)**	**Temp. (°F)**	**Relative Humidity (%)**
Mean	3.80	12.57	1.37	0.85	151.44	38.76	64.43
Hi	6.8	13.95	2.8	1.28	268.54	48.02	89
Low	1.9	10.78	0.6	0.67	99.50	30.56	31
Standard Deviation	1.28	0.99	0.44	0.13	20.62	5.27	17.47

Table 6. Statistical values for the concrete for the period November 12–13, 2007.

Concrete November 12–13 2007							
	LWIR DOLP (%)	**LWIR S0 (w/m^2)**	**MidIR DOLP (%)**	**MidIR S0 (w/m^2)**	**Atmospheric Radiation (w/m^2)**	**Temp. (°F)**	**Relative Humidity (%)**
Mean	2.86	14.08	0.85	1.12	133.21	51.51	85.28
Hi	4.40	15.24	2.70	1.32	240.05	60.26	94
Low	2.10	13.05	0.30	0.97	72.60	43.52	70
Standard Deviation	0.50	0.60	0.64	0.10	32.49	4.53	8.06

Table 7. Statistical values for the windshield for the period November 7–9, 2007.

Windshield November 7–9 2007							
	LWIR DOLP (%)	**LWIR S0 (w/m^2)**	**MidIR DOLP (%)**	**MidIR S0 (w/m^2)**	**Atmospheric Radiation (w/m^2)**	**Temp. (°F)**	**Relative Humidity (%)**
Mean	7.83	11.57	3.52	1.46	151.32	38.76	64.43
Hi	25.1	14.41	11.2	2.99	268.32	48.02	89
Low	2.5	8.76	0.8	1.09	99.42	30.56	31
Standard Deviation	6.52	1.46	2.40	0.37	20.60	5.27	17.47

Table 8. Statistical values for the windshield for the period November 12–13, 2007.

Windshield 12–13 2007							
	LWIR DOLP (%)	**LWIR S0 (w/m^2)**	**MidIR DOLP (%)**	**MidIR S0 (w/m^2)**	**Atmospheric Radiation (w/m^2)**	**Temp. (°F)**	**Relative Humidity (%)**
Mean	4.09	13.85	1.76	1.91	133.10	51.51	85.28
Hi	13.1	15.48	5.2	2.50	239.85	60.26	94
Low	1	11.91	0.3	1.61	72.54	43.52	70
Standard Deviation	2.78	0.81	1.56	0.25	32.46	4.53	8.06

Table 9. Statistical values for the tent for the period November 7–9, 2007.

Plastic Tent November 7–9 2007							
	LWIR DOLP (%)	**LWIR S0 (w/m^2)**	**MidIR DOLP (%)**	**MidIR S0 (w/m^2)**	**Atmospheric Radiation (w/m^2)**	**Temp. (°F)**	**Relative Humidity (%)**
Mean	5.23	11.43	1.79	0.76	151.32	38.76	64.43
Hi	17.6	16.98	14.3	1.95	268.32	48.02	89
Low	1.8	8.21	1.7	0.51	99.42	30.56	31
Standard Deviation	4.18	2.07	3.11	0.28	20.60	5.27	17.47

Table 10. Statistical values for the tent for the period November 12–13, 2007.

Plastic Tent November 12–13 2007							
	LWIR DOLP (%)	**LWIR S0 (w/m^2)**	**MidIR DOLP (%)**	**MidIR S0 (w/m^2)**	**Atmospheric Radiation (w/m^2)**	**Temp. (°F)**	**Relative Humidity (%)**
Mean	3.31	13.93	2.71	1.13	133.10	51.51	85.28
Hi	9.6	15.81	7.6	1.74	239.85	60.26	94
Low	0.7	11.71	0.4	0.87	72.54	43.52	70
Standard Deviation	1.65	0.95	2.27	0.22	32.46	4.53	8.06

Identified in each figure is the time and date at which the imagry was recorded as well as a day and night designation as defined by 0645 for sunrise and 1803 for sunset. Also shown for the November 7–9 period is a shaded interval designating light spotty periods of precipitation from approximately 0930 through 1915 on November 9, and a similarly shaded interval for the November 12–13 period designating stronger periods of rain from 0740 through 1000 on November 13. It should be noted that for the majority of both test periods, we experienced moderate to dense cloud cover with the exception of the evening hours on November 13. Intervals where there are no data points represent periods in which technical issues were experienced, either directly related with a particular polarimetric sensor or problems experienced during the data reduction and analysis portion of the study.

Data were intentionally plotted on a log based scale in order to show all measured parameters with their appropriate units, but more importantly to maintain and allow comparison of the "percent" change of a particular metric with another.

One obvious conclusion when reviewing the results of figures 5 through 14 is that, in general, the DOLP is always greatest in the LWIR when compared to MidIR. There are two primary reasons for this. First, it is known that ambient radiance due to the atmosphere is greater in the MidIR compared to the LWIR where the atmosphere appears more quiescent. This additional radiance present in the MidIR becomes partially linearly polarized upon reflection from the surface of the object being examined. The polarization state of the reflected energy is known to be orthogonal to the polarization state of the energy emitted for the thermal object (*2*). The two combine destructively resulting in a net reduction of the recorded DOLP at the sensor. This effect can be seen most readily in the data sets comprised of target surfaces that are oriented upward towards the sky, i.e., the windshield, plastic tarp, and the concrete surfaces. The general trend shown in the figures 5 through 14 is that as the ambient levels of atmospheric radiance increase (usually associated with additional H_2O content), the measured MidIR DOLP decreases since the

increasing ambient reflected energy serves to reduce the net linear component of polarization recorded. Because the degree of ambient loading is much less in the LWIR, this superposition effect is less noticeable. In addition to the variation observed due to atmospheric water vapor content, the MidIR DOLP also tended to vary with rain. This is most likely due to the increased reflectivity of the various surfaces as they became coated with water (*3*).

Adding to the difference in the measured values of the DOLP between LWIR and MidIR is the fact that a given surface "appears" more specular or smooth for the longer wavelengths and it is well known that optically smooth surfaces better preserve linear polarization states upon reflection and/or emission (*4*). An object's surface is determined to be optically "smooth" or "rough" according to the ratio of an average surface roughness parameter (usually on the order of microns) and the wavelength of light being considered. As a result, because the MidIR wavelengths (3–5 microns) are comparable to typical surface roughness values, radiation in this waveband is more susceptible to depolarization upon reflection. On the other hand, typical surface roughness appears relatively small when the wavelengths of the radiation increases by a factor of 2 or 3, i.e., in the LWIR (8–14 microns). These surfaces are more specular in the LWIR, and therefore, preserve and induce linearly polarized light upon reflection.

In figures 5 through 14, there is a spread, or scatter, associated with certain calculated DOLP values. This variation is most noticeable for the two most specular surfaces, i.e., the windshield and plastic tent surface. Both surfaces are effective reflectors and are oriented towards the most dynamic source of reflected energy, i.e., the cloud covered sky. The variance in their DOLP measurements is understandable since it is strongly linked to the reflected radiance present in the environment. Conversely, those surfaces that are more diffuse, or Lambertian, exhibit nearly constant values of DOLP throughout a given diurnal cycle.

There is yet another factor effecting the variance of a polarimetric data product to consider. Scatter, or noise, is often introduced/magnified through the computation process required to calculate a given parameter. As an example, in order to calculate the DOLP value (as defined in equation 4), the algebraic process involves no fewer than five mathematical operations. As a result, the normal uncertainty associated with any measurable quantity (in this case, radiance values deduced from an IR image) is propagated through equation 4 and is effectively amplified resulting in additional variance within the normal trend of the DOLP parameter. Although the DOLP is a useful and commonly used polarimetric metric, a simpler expression may suffice, such as just S_1 or S_2, for example.

4. Conclusion

We have presented radiometric and polarimetric calibrated imagery recorded in both the MidIR and LWIR as a function of diurnal variation over several multiday periods. The two camera systems used in the study differed significantly in design. The LWIR polarimetric sensor utilizes a spinning achromatic retarder and is best suited for static scenes, while the MidIR system is based on a DOA design and is capable of recording polarimetric imagery of targets that are rapidly moving. The meteorological parameters measured during the study included temperature, relative humidity, wind speed/direction, precipitation, and ambient atmospheric IR loading.

The key observations in this study were as follows:

- The thermal polarimetric response appears slightly stronger in the LWIR compared to the MidIR. The ranges in DOLP values for the regions of interest in this study were typically 0.5–4% in the MidIR and 3–8% in the LWIR.
- The polarimetric signatures in the MidIR are more susceptible to diurnal effects such as cloud cover and atmospheric H_2O content.
- Specular reflecting surfaces produce the greatest variation in the IR polarimetric signals.
- Most manmade materials encountered tend to be relatively diffuse (Lambertian) and are shown to be reasonably stable throughout the diurnal cycles considered here.

It was concluded that simpler data products, such as S_1 and S_2, may be just as effective as the DOLP at producing useful polarimetric information needed for certain applications. One such application is the enhancement of targeting and tracking capabilities of objects of interest that are embedded in complex scenes. Since most manmade objects of interest have pronounced geometric features oriented with respect to the horizontal and vertical axis, e.g., buildings, vehicles, and other structures, a simple polarimetric product, such as an S_1 image (which highlights the amount of vertically vs. horizontally polarized light), may suffice and be just as effective as a DOLP image in suppressing clutter and improving the contrast between the object of interest and the background.

References

1. Pezzaniti, J. L. *System Users Manual: Fast MWIR Imaging Polarimetry*, Contract number DAAD17-03-C-0109, 2007.
2. Sandus, O. A Review of Emission Polarization. *Appl. Opt.* **1965**, *4*, 12.
3. Tyo, J. S.; Goldstein, D. L.; Chenault, D. B.; Shaw, J. A. Review of passive imaging polarimetry for remote sensing applications. *Appl. Opt.* **2006**, *45*, 22.
4. Gurton, K. P.; Dahmani, R. Effect of surface roughness and complex indices of refraction on polarized thermal emission. *Appl. Opt.* **2005**, *44*, 26.

Acronyms

AD	analog-to-digital
BaF_2	barium fluoride
DOA	division-of-aperture
DOLP	degree-of-linear polarization
FOV	fields-of-view
FPA	focal-plane array
InSb	indium antimonide
IR	infrared
LOS	line-of-sight
LWIR	long-wave IR
MCT	mercury cadmium telluride
MidIR	mid-wave IR
NUC	nonuniformity corrections
ROI	regions-of-interest

No. of Copies	Organization
1 (PDF ONLY)	ADMNSTR DEFNS TECHL INFO CTR ATTN DTIC OCP (ELECTRONIC COPY) 8725 JOHN J KINGMAN RD STE 0944 FT BELVOIR VA 22060-6218
1	DARPA ATTN IXO S WELBY 3701 N FAIRFAX DR ARLINGTON VA 22203-1714
1 CD	OFC OF THE SECY OF DEFNS ATTN ODDRE (R&AT) THE PENTAGON WASHINGTON DC 20301-3080
1	ADVANCED TECHNOLOGIES DIRECTORATE SPACE & MISSILE COMMAND ATTN D LIANOS PO BOX 1500 HUNTSVILLE AL 35805
1	US ARMY RSRCH DEV AND ENGRG CMND ARMAMENT RSRCH DEV AND ENGRG CTR ARMAMENT ENGRG AND TECHNLGY CTR ATTN AMSRD AAR AEF T J MATTS BLDG 305 ABERDEEN PROVING GROUND MD 21005-5001
1	US ARMY TRADOC BATTLE LAB INTEGRATION & TECHL DIRCTRT ATTN ATCD B 10 WHISTLER LANE FT MONROE VA 23651-5850
2	PICATINNY ARSENAL ATTN L E ROTH ATTN M WOOLLEY BLDG PICATINNY ARSENAL NJ 07806-5000
1	US ARMY ABERDEEN TEST CENTER ATTN CSTE DT AT WC A F CARLEN 400 COLLERAN ROAD ABERDEEN PROVING GROUND MD 21005-5009

No. of Copies	Organization
1	US ARMY CECOM RDEC NVESD ATTN J HOWE 10221 BURBECK RD STE 430 FT BELVOIR VA 22060-5806
1	US ARMY INFO SYS ENGRG CMND ATTN AMSEL IE TD F JENIA FT HUACHUCA AZ 85613-5300
1	US ARMY NVESD ATTN AMARD CER NV ST ICT M SCHATTEN 10221 BURBECK RD FT BELVOIR VA 22060-5806
1	COMMANDER US ARMY RDECOM ATTN AMSRD AMR W C MCCORKLE 5400 FOWLER RD REDSTONE ARSENAL AL 35898-5000
1	US ARMY RDECOM AMRDEC ATTN AMSRD-AMR-SG-IP H F ANDERSON BLDG 5400 REDSTONE ARSENAL AL 35809
1	US ARMY RDECOM ARDEC ATTN AMSRD AAR MEF S J ROMANO BLDG 704 PICATINNEY ARSENAL NJ 07806-5000
1	AIR FORCE RSRCH LAB AFRL/MNGG ATTN D R SNYDER 101 WEST EGLIN BLVD EGLIN AFB FL 32542-6810
1	US GOVERNMENT PRINT OFF DEPOSITORY RECEIVING SECTION ATTN MAIL STOP IDAD J TATE 732 NORTH CAPITOL ST NW WASHINGTON DC 20402
1	ARROW PROGRAM OFFIC ATTN MDA AW S CHITWOOD 106 WYNN DR HUNTSVILLE AL 35805

No. of Copies	Organization
1	NATIONAL SIGNATURES PROGRAM ATTN C JONES 11781 LEE JACKSON MEMORIAL HWY FAIRFAX VA 22033-3309
1	US ARMY RSRCH LAB ATTN AMSRD ARL CI OK TP TECHL LIB T LANDFRIED BLDG 4600 APG MD 21005-5066
1	DIRECTOR US ARMY RSRCH LAB ATTN AMSRD ARL RO EV W D BACH PO BOX 12211 RESEARCH TRIANGLE PARK NC 27709
17	US ARMY RSRCH LAB ATTN AMSRD ARL CI E P CLARK (1) ATTN AMSRD ARL CI ES A RAGLIN (1) ATTN AMSRD ARL CI ES D LIGON (1) ATTN AMSRD ARL CI ES K GURTON (10s) ATTN AMSRD ARL CI ES M FELTON (1) ATTN AMSRD ARL CI OK T TECHL PUB (1 CD) ATTN AMSRD ARL CI OK TL TECHL LIB (1 CD) ATTN IMNE ALC IMS MAIL & RECORDS MGMT (1 CD) ADELPHI MD 20783-1197
Total:	38 (1 PDF, 36 HCs, 1 CD)

INTENTIONALLY LEFT BLANK.